DOI: 10.13009/EUCASS2022-4454
9TH EUROPEAN CONFERENCE FOR AERONAUTICS AND SPACE SCIENCES (EUCASS)

# DSMC Computations of Inflatable Aerodynamic Decelerators for CubeSats

*Rodrigo Cassineli Palharini*, Diego Rioseco Olave*, and Nicolas Caqueo Jara**
**Department of Mechanical Engineering, Universidad Técnica Federico Santa María, San Joaquín, Santiago, Chile*

## Abstract
During atmospheric reentry, a high temperature shock wave is formed in front of the vehicle. In order to protect the crew and experiments, external insulation materials composed by a rigid aeroshell have been used. Reinforced carbon-carbon, low- and high-temperature reusable surface insulation tiles, and felt reusable surface insulation blankets are just some of the materials that have been employed to protect the spacecraft during the harsh reentry environment. With the advance of manufacturing processes and the development of flexible high-temperature materials, a new trend has emerged: the use of Inflatable Aerodynamic Decelerator (IAD) as thermal protection system. IADs technology is of great interest because such devices inflate to their full size in space and are not directly constrained by the launch vehicle payload shroud diameter like rigid aeroshells, nor inflation conditions like parachutes. They can provide both deceleration and thermal protection capabilities decreasing the entry vehicle complexity, providing a more reliable and efficient way to deliver payloads onto the surface of a planet. Another benefit is that IADs can be deployed either exo-atmospherically or during the hypersonic phase of flight, which allows an increased timeline before touch-down. In addition, this system can be used to protect CubeSats during the reentry making them reusable, further decreasing their costs. The main goal of this work is to investigate the altitude effect during the reentry phase of a cubeSat with inflatable aerodynamic decelerator. According to the results, the altitude had a significant impact on the properties along the stagnation line and shock wave structure

## 1. Introduction

One of the most challenging problem of planetary exploration is design and development of a vehicle capable of surviving an atmospheric entry. Special care has to be taken so that the entry vehicle can decelerate sufficiently and dissipate the large heat load experienced from traveling through the atmosphere. This is typically accomplished using a rigid thermal protection system (TPS), however, space missions which include heavy payloads require larger drag devices to decelerate and safely land the vehicles. This can be achieved either by increasing the diameter of the aeroshell, using a larger parachute or developing a different entry-descend-landing (EDL) system [1].
Increasing the diameter of the aeroshell is not feasible since it need to be packaged in the rocket payload shroud, limiting the entry vehicle maximum area to 5 $m^2$ . An alternative solution is to increase drag using aerodynamic decelerators. The most common aerodynamic decelerators have historically been parachute systems. Parachutes have flown on manned mission including Apollo, which used both high altitude drogue parachutes for stabilization and main parachutes to achieve a safe terminal velocity. However, complications in supersonic parachute inflation and their inability to survive the extreme hypersonic heating conditions place substantial limitations on parachute's abilities to land heavy payloads [1].
One of the proposed EDL technology is the Inflatable Aerodynamic Decelerator (IAD) [2]. IADs are of interest for this mission class because such devices inflate to their full size in space and are not directly constrained by the launch vehicle payload diameter. They can provide both deceleration and thermal protection capabilities and potentially decrease the entry vehicle complexity, providing a more reliable and efficient way to deliver payloads onto the surface of a planet. Another benefit is that IADs can be deployed either exo-atmospherically or during the hypersonic phase of flight. Reasons for the use of inflatable structures range from their low cost over exceptional packaging efficiency, deployment reliability, and low storage volume to low weight ratio. Especially the aspect of the low manufacturing costs makes inflatable structure a prestigious field for university based research and projects or small satellite missions [3]. Figure 1 shows the flight concept of an IAD configuration.

DOI: 10.13009/EUCASS2022-4454



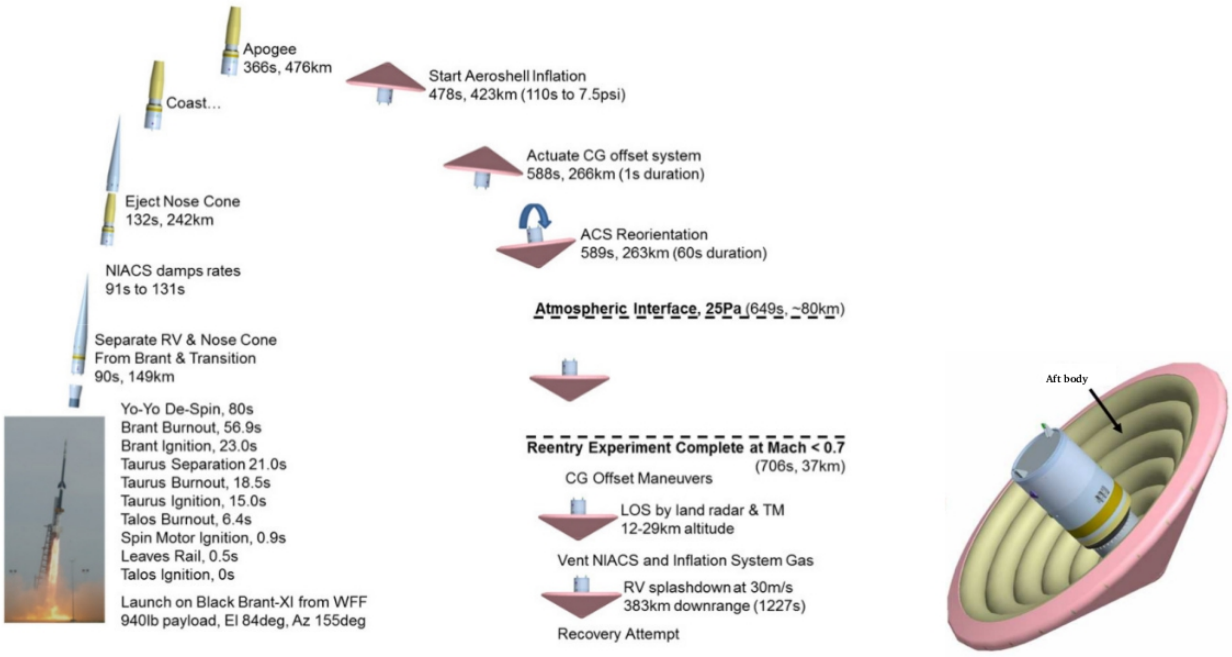


**Figure 1:** a) Schematic of an IAD employed in the Re-entry Vehicle Experiment-3 (IRVE-3) and b) amplified view IRVE-3 [4].

Inflatable vehicles, which were first proposed in the 1960s, afford remarkable advantages, such as lower-ballistic coefficient flight during atmospheric reentry, low weight and volume, and large deceleration when compared with rigid aeroshells. NASA, the European Space Agency (ESA), and Japan Aerospace Exploration Agency (JAXA) have conducted several studies and demonstration flights of such vehicles. In order to operate safely, a few numerical and experimental studies have been conducted aimed at understanding the aerothermodynamics of IAD systems [5-10].
Accurate prediction and identification of the key factors that impact the thermal response of the IAD. In this way, in order to gain a better understanding to develop and design IAD systems for cubeSats, numerical simulations were conducted using the direct simulation Monte Carlo technique. The impact of non-reactive hypersonic gas flows over a cubeSat with IAD system was investigated at different altitudes.

## 2. The DSMC method

The DSMC technique instructs particles to move and collide using kinetic-theory considerations in order to accurately capture non-equilibrium gas behavior. DSMC considers molecular collisions using stochastic, rather than deterministic, procedures over a time step which is a small fraction of the mean collision time. Each DSMC particle represents a large number of real gas molecules. The decoupling of particle ballistic motion and particle collisions greatly improves the computational efficiency of DSMC in comparison with other particle methods such as molecular dynamics (MD). The computational domain is divided into either a structured or unstructured grid of cells, with each cell of a dimension that is a small fraction of the local mean free path size ($\lambda$). The cells are then utilized to select particles for collisions on a probabilistic basis, and they are also used for sampling the macroscopic flow properties. Intermolecular collisions are handled probabilistically using phenomenological models which are designed to reproduce real fluid behavior when the flow is examined at the macroscopic level. The DSMC technique has been shown to provide a solution to the Boltzmann equation as the number of simulated particles tends toward the true value within the flow field [11]. The DSMC approach is currently the dominant numerical method for rarefied gas flow applications [12-13].
The DSMC code used in this investigation is called dsmcF oam. The code has been written within the framework of the open-source C++ CFD toolbox OpenFOAM [14]. The main features of the dsmcFoam code include the capability to perform both steady and transient DSMC simulations for multi-species conditions, to model arbitrary 2D/3D geometries using unstructured polyhedral meshes, and unlimited parallel processing. The original version of dsmcF oam determines intermolecular collisions for polyatomic species using the variable hard sphere (VHS) model [12] and applies the phenomenological Larsen-Borgnakke model to distribute post-collision energy between the translational, rotational, and vibrational modes [12]. A series of successful benchmark trials have been carried out which have validated the dsmcF oam code for non-reacting and reacting gas flows [13, 15-17].

DOI: 10.13009/EUCASS2022-4454



## 3. Computational parameters

In this section, the computational the IAD geometrical parameters and freestream condition used during the simulations are explained in detail.

### 3.1 IAD geometric parameters

The IAD consists of a cylindrical structure containing all the subsystems necessary for the on-orbit mission and for the re-entry phase, umbrella-like frameworks, off-the-shelf ceramic fabrics for the conical deployable heat shield and available ceramic materials for the rigid hemispherical nose [18]. The IAD configurations considered in the present investigation are shown in Figure 2. The diameter (D) of the inflated system considered in this work is 1080 mm, and cylindrical body length (L) of 600 mm [18].

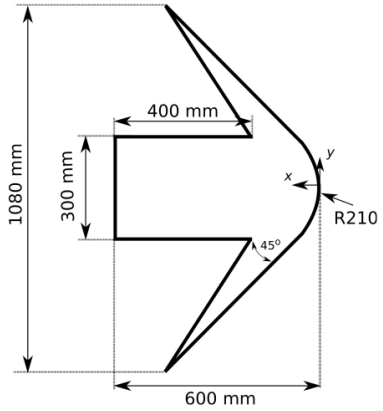


**Figure 2:** Geometric parameters of the IAD configuration.

### 3.2 Freestream conditions

The flow over IADs was modeled employing the dsmcFoam-QK code developed by the "James Weir Fluids Laboratory" at University of Strathclyde. Freestream flow conditions experienced by the IAD are tabulated in Table 1 [19]. In the present work, the reentry velocity ($U_\infty$) and the surface temperature T w are assumed to be constant, 7000 m/s and 1000 K, respectively. The wall temperature is chosen to be representative of the surface temperature near the stagnation point.

**Table 1:** Freestream flow conditions [19].

| Altitude (km) | Velocity (m/s) | Density (kg/m$^3$) | N. Density (m$^{-3}$) | Temperature (K) | Pressure (N/m$^2$) | MFP (m) |
|---|---|---|---|---|---|---|
| 115 | 7000 | $4.289\times10^{-8}$ | $9.6466\times10^{17}$ | 300.0 | $4.008\times10^{-3}$ | 1.830 |
| 110 | 7000 | $9.709\times10^{-8}$ | $2.1334\times10^{18}$ | 240.0 | $7.104\times10^{-3}$ | 0.762 |
| 105 | 7000 | $2.325\times10^{-7}$ | $4.9881\times10^{18}$ | 208.8 | $1.428\times10^{-2}$ | 0.312 |
| 100 | 7000 | $5.604\times10^{-7}$ | $1.1791\times10^{19}$ | 195.1 | $3.011\times10^{-2}$ | 0.130 |
| 95 | 7000 | $1.393\times10^{-6}$ | $2.8947\times10^{19}$ | 188.4 | $7.596\times10^{-2}$ | 0.052 |

The overall Knudsen number, K n , is defined as the ratio of the molecular mean free path (MFP), λ, in the freestream gas to a characteristic dimension of the flowfield. According to Bird [12], the region defined by 0.01 < K n <10 is referred as the slightly rarefied and transition flow regimes, where not only the gas-surface collisions but also the intermolecular collisions are important. In the transition flow regime, viscosity, heat conduction, chemical relaxation and diffusion processes are important. In this context, the velocity distribution function may deviate from

DOI: 10.13009/EUCASS2022-4454



the Maxwell distribution function, which results in a thermodynamic nonequilibrium gas flow. Assuming the IAD radius as the characteristic length, the Knudsen numbers correspond to 8.7, 3.6, 1.5, 0.6 and 0.2 for altitudes of 115, 110, 105, 100, and 95 km, respectively. In the transition flow regime, the aerodynamic heating and the forces acting on the vehicle surfaces are very sensitive to the degree of rarefaction.

## 4. Validation of the computational code

In order to valdate the dsmcFoam code used in the present investigation, the blunt cone model has been chosen as a test case [20-24]. Experimental investigations was carried out by the Center National de la Recherche Scientific (CNRS) at the SR3 low-density wind tunnel using a nitrogen flow over a 70° blunt cone, representative of Mars Pathfinder probe [24].

The experiments performed at SR3 wind tunnel considered three cases setup with the aim of determining flowfield structure, surface properties and forces acting on the probe. In the first experiment, density distribution was mesured over the Mars Pathfinder probe. During the experiment the probe wall was kept at 290 K and it was estimated a mesurement precision of 10%, except in the region that encompasses the shock wave, which is characterized by high density gradients and therefore there is a greater uncertainty. The results obtained by CNRS during the rarefied wind tunnel experiments were compared with those computed by the dsmcFoam and the DSMC Analysis Code (DAC) codes [24].

The computational simulations performed by dsmcFoam code employed the Larsen-Borgnakke phenomenological model [25] to control the energy exchange between translation and rotation modes. Molecular collisions were modeled using the Variable Hard Sphere (VHS) model [12], and the non-time counter (NTC) collision sampling technique [12]. The geometry was positioned at a zero angle of attack, which allows simulating a quarter of the problem. The computational domain extends 0.02 [m] upstream of the probe and 0.08 [m] in the Y and -Z directions. The boundary condition on the surface of the geometry is a diffuse gas-surface interaction with complete thermal accommodation at the surface temperature. The wall temperature was set to 290 K during the simulations. For the validation process of the dsmcFoam code, the computational mesh was made up of 3.96 million cell with an average of 8.23 simulated particles per cell. The mesh is mostly hexahedral and uniform with a cell size less than a third of the mean free. In addition, it was used a time step of $1.0 \times 10^{-8}$ [s] and a total of 300,000 sampling iterations to conclude the simulation.

In Figure 3, the normalized density distribution ($\rho/\rho_\infty$) obtained during the experiments was compared with dsmcFoam and DAC computations. Accordint to this plot, it is noticed a good agreement between the results obtained with the dsmcFoam and DAC codes with the experimental data. In this scenario, the dsmcFoam code is considered validated for the intented purpose.

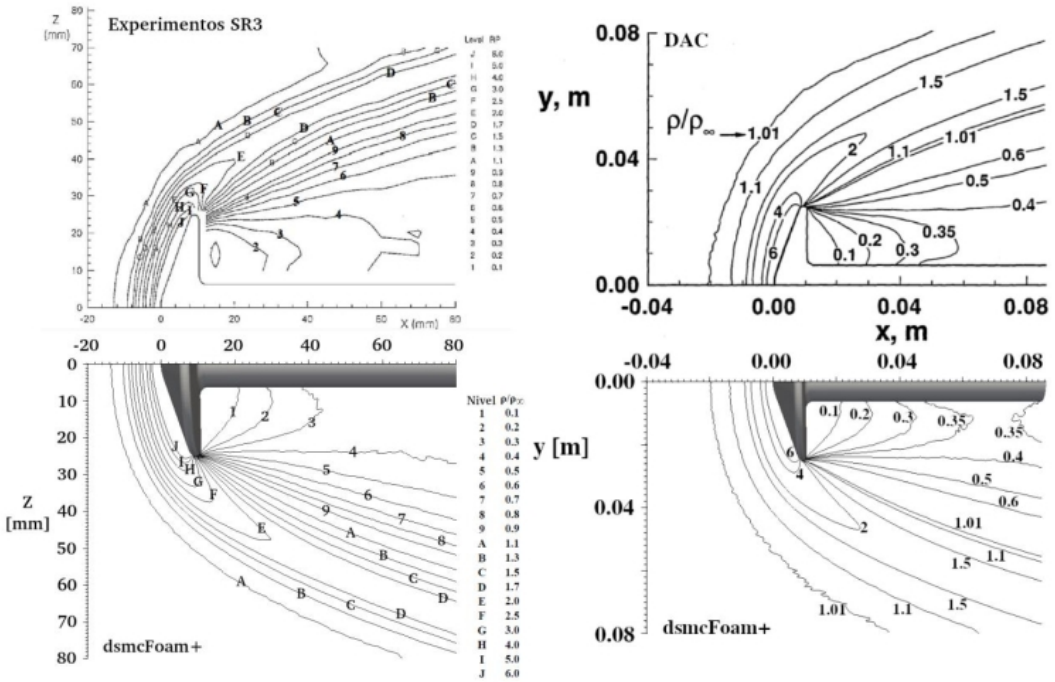


**Figure 3:** Comparison of the nomalized density distribution ($\rho/\rho_\infty$) between the experimental results of CNRS and the numerical ones obtained with the dsmcFoam code.

DOI: 10.13009/EUCASS2022-4454



# 5. Computational results and discussions

## 5.1 Translational Temperature Field

The influence of altitude on the translational temperature distributions is shown in Figure 4. The translational temperature is measured along the stagnation streamline which vary from the computational domain inlet to the capsule stagnation point. According to the temperature distribution, it clear seen that the shock wave formed upstream of the IAD at 115 km altitude is more diffuse when compared to those presented at 95 km altitude. The main characteristic of a diffuse shock wave is the wide temperature profile. As the vehicle moves towards Earth's surface, the temperature profile along the stagnation tends to be thinner and to move close to the vehicle surface. In addition, for the lowest altitude considered, it is observed a significant increase on the peak of translational temperature.

In order to illustrate in a better way the influence of altitude in the translational temperature, temperature contour maps around the IAD are presented in Figure 5 for the altitudes considered in this study. According to Figure 5, it is observed a diffuse shock wave formation upstream of the vehicle at 115 km altitude. This shock wave expands around the vehicle and its thickness is larger than to those observed for the 95 km altitude. At 105 km altitude, it is clear noticed a decrease on the shock wave thickness due the increase of atmospheric density. Finally, the translational temperature contour at 95 km altitude, the shock wave is closer to the vehicle stagnation point and a increase of the peak temperature is observed when compared with the computational results obtained at 115 km altitude.

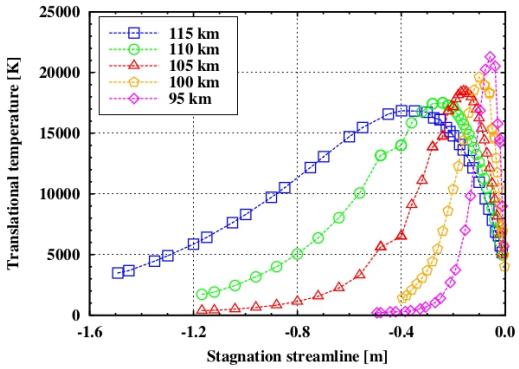


**Figure 4:** Influence of altitude on the translational temperature distribution along the stagnation streamline.

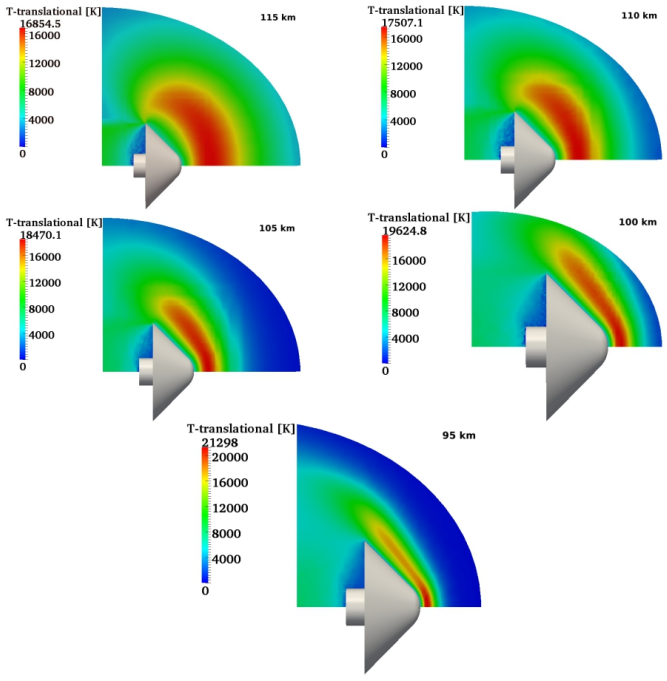


**Figure 5:** Influence of altitude on the translational temperature contours around the IAD.

DOI: 10.13009/EUCASS2022-4454



## 5.2 Number Density Field

The impact of the altitude on the number density distribution along the stagnation stream line is showed in Fig. 5. According to Figure 6, the atmospheric number density is quite low at the computational domain inlet, however, as the gas particles moves towards the vehicle surface, it is noticed a peak in the number density close to the vehicle stagnation point. The particles that are reflected from the vehicles surface collides with incoming freestream molecules promoting an increase on the number density around the vehicle heat shield. This phenomenon is clearly observed at the number density contours at Figure 7. As the vehicle moves through thicker layers of Earth's atmosphere, it is noticed a higher particles concentration close to the surface. The increase on the particles density, may lead to an increase on the particles collision frequency which in turn could excite the internal energy level of the molecules. High temperature shock waves and high number density are the key factor for the production of chemical reactions during the atmospheric reentry.

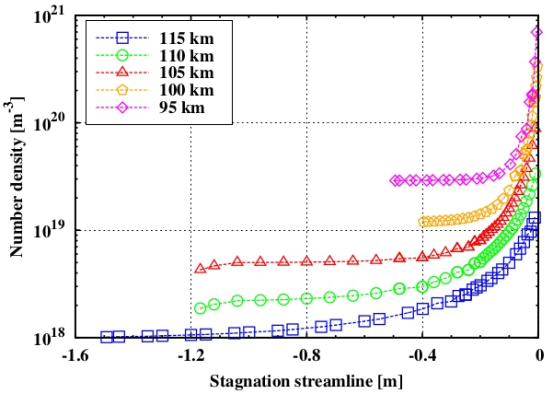


**Figure 6:** Influence of altitude on the number density distribution along the stagnation streamline of IAD.

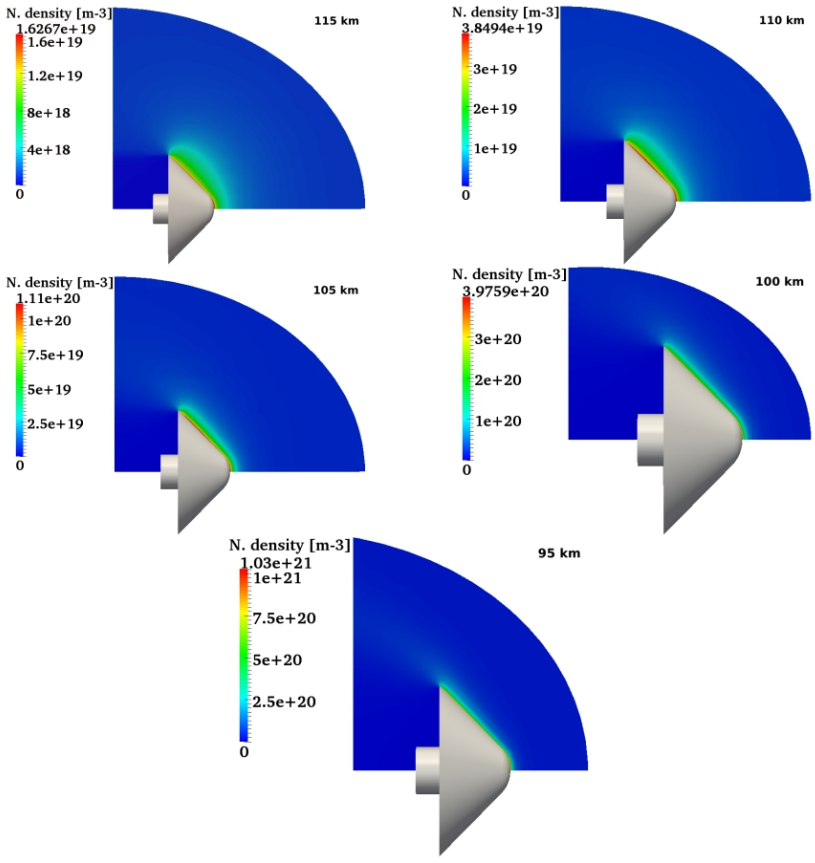


**Figure 7:** Influence of altitude on the number density contours around the IAD.

DOI: 10.13009/EUCASS2022-4454



### 5.3 Pressure Field

In similar approach, to the temperature and number density, Figure 8 presents the pressure distribution along the stagnation streamline for altitudes ranging from 115 to 95 km. From this plot, it is observed that the pressure distribution follow the same trend and the number density, i.e., the pressure is low far from upstream the stagnation point and increase to a maximum value at the stagnation point (X = 0.0). In addition, the maximum stagnation pressure for the 95 km case is fifth times higher to those found at 115 km altitude. The pressure contours around the IAD are presented in Figure 9 for the altitudes considered in this work. The highest pressure is found close to the vehicle surface and as the flow expand into the wake region pressure reached minimum values. At the IAD forefront, the pressure variation w.as 0.97, 2,32, 6,25, 18.56, and 53.02 Pa in the altitudes of 115, 110, 105 km, 100, and 95 respectively.

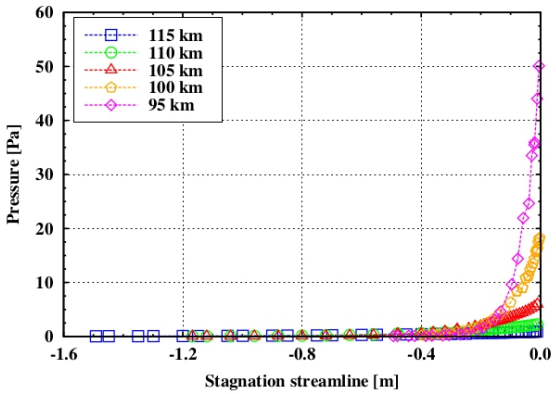


**Figure 8:** Influence of altitude on the number density distribution along the stagnation streamline.

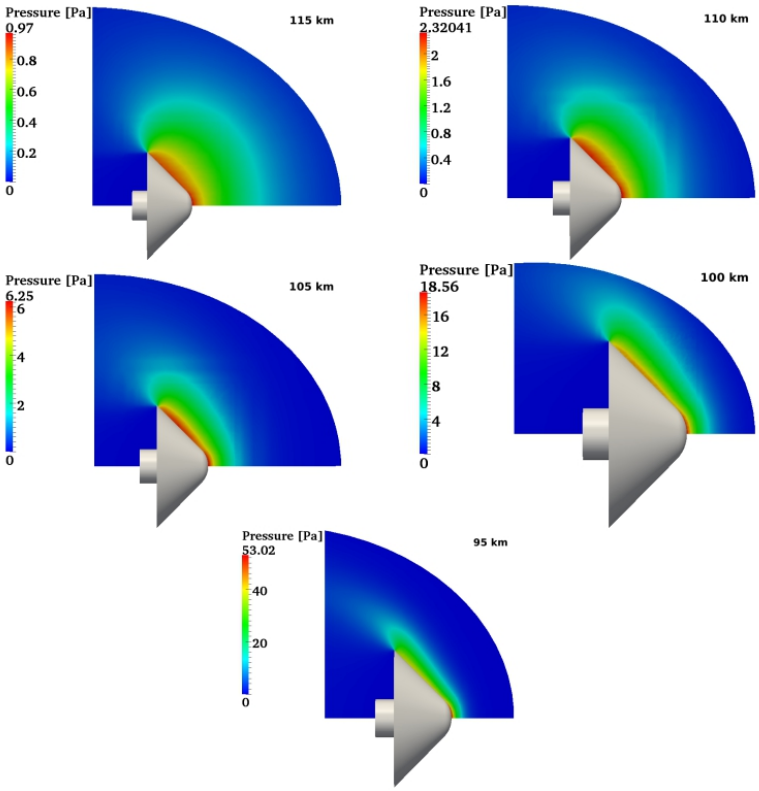


**Figure 9:** Influence of altitude on the pressure contours around the IAD.

DOI: 10.13009/EUCASS2022-4454



### 5.4 Velocity Field

The velocity distribution along the stagnation streamline for different reentry altitudes is shown in Figure 10. According to results, the velocity is high at the inlet and decrease to a minimum value at the stagnation point. In addition, it also observed that the decrease on velocity occurs faster for the 95 km altitude. In contrast, the velocity profiles for the simulations performed at 115 km altitude decreases slowly when compared with the 110, 105 and 100 km. This behavior is due to the small number of collisions between the particles at the highest altitudes. Finally, the velocity contour maps are presented in Figure 11 for each altitude considered in this work. In this set of plots, it is evident the diffuse nature of the shock wave at the higher altitude and as the vehicle reaches denser parts of the atmosphere, the smallest values of velocity are found close to the vehicle surface.

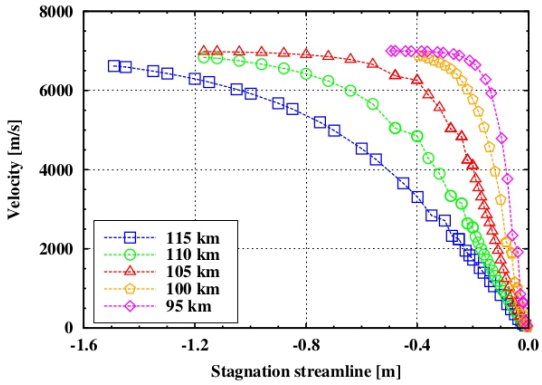


**Figure 10:**. Influence of altitude on the velocity distribution along the stagnation streamline of IAD.

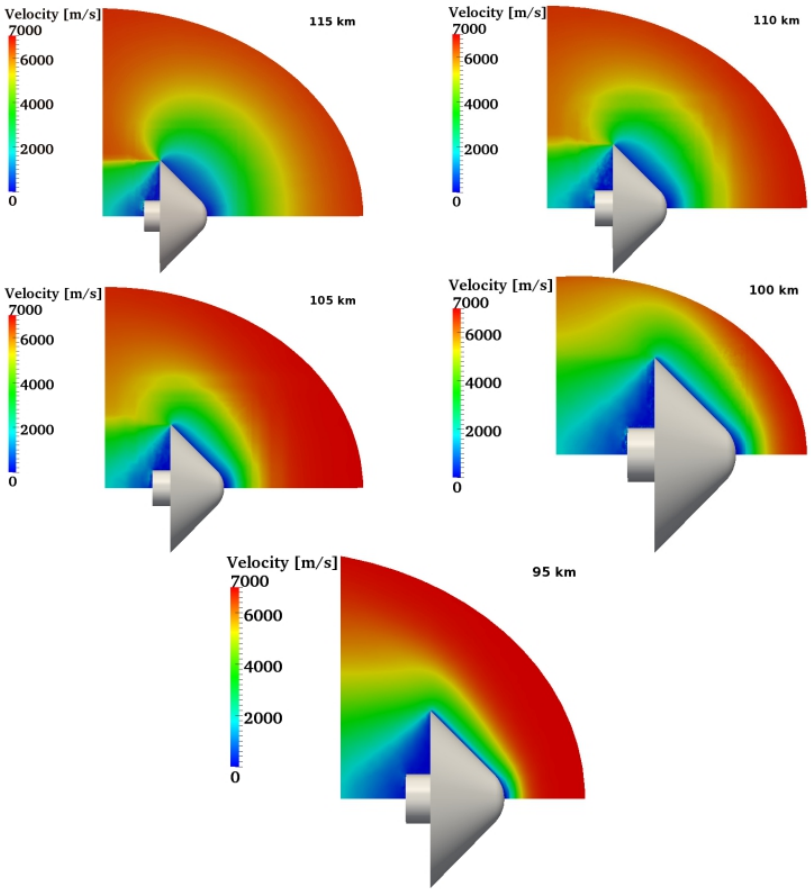


**Figure 11:** Influence of altitude on the velocity contours around the IAD.

DOI: 10.13009/EUCASS2022-4454



## 6. Conclusions

In the present investigation, the Direct Simulation Monte Carlo technique was employed to investigate a hypersonic rarefied gas flow around a cubeSat with inflatable aerodynamic decelerator. The freestream conditions considered in this work corresponded to those found in the Earth atmosphere from 115 km to 95 km altitude. The main goal was to investigate the influence of the altitude on the primary properties distribution along the stagnation streamline and shock wave structure.

According to the computed results, it was observed that the altitude has a significant influence on the shock wave structure and in the peak of translational temperature. As the vehicle descent towards Earth's surface, the atmospheric density increases and more collisions between the air molecules and the IAD wall are observed. Consequently, it was noticed a significant augmentation on the shock wave temperature and a decrease on the shock wave structure.

## 7. Acknowledgements

The authors gratefully acknowledge the partial support for this research provided by Agencia Nacional de Investigación y Desarrollo (ANID), under the Research Grant No. 11190068. Research carried out using the computational resources of the Center for Mathematical Sciences Applied to Industry (CeMEAI) funded by FAPESP (Grant No. 2013/07375-0). In addition, the authors would like to thank the support of the Valparaíso Scientific and Technological Center (Grant No. ANID PIA/APOYO AFB180002).

## References

[1] Brune, A.J., Hosder, S., Edquist, K.T. and Tobin, S.A., 2016. "Uncertainty analysis of thermal protection system response of a hypersonic inflatable aerodynamic decelerator". In 46th AIAA Thermophysics Conference. Washington, D.C., AIAA 2016-3535.

[2] Hughes, J., Dillman, R.A., Starr, B.R., Stephan, R.A., Lindell, M.C., Player, C.J. and Cheatwood, D.F.M., 2005. "Inflatable re-entry vehicle experiment (irve) design overview". AIAA Journal.

[3] Walther, S., Thaeter, J., Reimers, C., Marraffa, L., Pitchkhadze, K. and Alexashkin, S., 2003. "New space application opportunities based on the inflatable reentry and descent technology (irdt)". In AIAA/ICAS International Air and Space Symposium and Exposition: The Next 100 Year. Dayton, Ohio.

[4] Corso, J.A.D., Cheatwood, F.M., Bruce III, W.E. and Hughes, S.J., 2011. "Advanced high-temperature flexible tps for inflatable aerodynamic decelerators". In 21st AIAA Aerodynamic Decelerator Systems Technology Conference and Seminar. Dublin, Ireland.

[5] Zuppardi, G., Savino, R. and Mongelluzzo, G., 2016. "Aero-thermo-dynamic analysis of a low ballistic coefficient deployable capsule in earth re-entry". Acta Astronautica, Vol. 127, pp. 593–602.

[6] Iacovazzo, M., Carandente, V. and Savino, R. Zuppardi, G., 2015. "Longitudinal stability analysis of a suborbital re-entry demonstrator for a deployable capsule". Acta Astronautica, Vol. 106, pp. 101–110.

[7] Carandente, V., Savino, R., D'Oriano, V. and Fortezza, R., 2015. "A study on earth re-entry capsules with deployable aerobrakes for recoverable microgravity experiments". Microgravity Science and Technology, Vol. 27, pp. 181–191.

[8] Andrews, J., Watry, K. and Brown, K., 2011. "Nanosat de-orbit and recovery system to enable new missions". In 25th Annual AIAA/USU Conference on Small Satellites.

[9] Reynier, P. and Evans, D., 2009. "Postflight analysis of inflatable reentry and descent technology blackout during earth reentry". Journal of Spacecraft and Rockets, Vol. 6, No. 4, pp. 800–809.

[10] Yamada, K., Akita, D., Sato, E., Suzuki, K., Narumi, T. and Abe, T., 2009. "Flare-type membrane aeroshell flight test at free drop from a balloon". Journal of Spacecraft and Rockets, Vol. 46, No. 3, pp. 606–614.

[11] Wagner, W.A., 1992. "A convergence proof for Bird's direct simulation Monte Carlo method for the Boltzmann equation". Journal of Statistical Physics, Vol. 66, pp. 1011–1044.

[12] Bird, G., 1994. Molecular Gas Dynamics and the Direct Simulation of Gas Flows. Clarendon, Oxford.

[13] Bird, G.A., 2011. "The QK model for gas-phase chemical reaction rates". Physics of Fluids, Vol. 23, No. 10, p. 106101.

[14] OpenFOAM Foundation, 2022. "http://www.openfoam.org/".

[15] Scanlon, T.J., Roohi, E., White, C., Darbandi, M. and Reese, J.M., 2010. "An open source, parallel, DSMC code for rarefied gas flows in arbitrary geometries". Computers & Fluids, Vol. 39, pp. 2078–2089.

[16] Scanlon, T.J., White, C., Borg, M.K., Palharini, R.C., Farbar, E., Boyd, I.D., Reese, J.M. and Brown, R.E., 2015. "Open- source direct simulation Monte Carlo chemistry modeling for hypersonic flows". AIAA Journal, Vol. 53, No. 6, pp. 1670–1680.

DOI: 10.13009/EUCASS2022-4454



[17] Palharini, R.C., White, C., Scanlon, T.J., Brown, R.E., Borg, M.K. and Reese, J.M., 2015. Benchmark numerical simulations of rarefied non-reacting gas flows using an open-source DSMC code. Computers & Fluids, 120, pp.140-157.
[18] Carandente, V., Zuppardi, G. and Savino, R., 2014a. "Aerothermodynamic and stability analyses of a deployable re-entry capsule". Acta Astronautica, Vol. 93, pp. 291–303.
[19] NOAA/NASA/USAF, 1976. "U. S. Standard atmosphere". U.S. Government Printing Office.
[20] Muylaert J, et al. Hypersonic experimental and computational capability, improvement and validation. North Atlantic Treaty organization, Advisory Group for Aerospace Research & Development; 1998.
[21] J. Allègre, et al. Experimental Rarefied Density Flowfields at Hypersonic Conditions over 70-Degree Blunted Cone. J Spacecraft Rockets 1997; 34(6): 714–718.
[22] J. Allègre, et al. Experimental Rarefied Aerodynamic Forces at Hypersonic Conditions over 70-Degree Blunted Cone. J Spacecraft Rockets 1997; 34(6): 719–723.
[23] J. Allègre, et al. Experimental Rarefied Aerodynamic Heat Transfer at Hypersonic Conditions over 70-Degree Blunted Cone. J Spacecraft Rockets 1997; 34(6): 724–728.
[24] Moss JN, Dogra VK, Wilmoth RG. DSMC simulations of Mach 20 nitrogen flows about a 70-degree blunted cone and its wake. Tech. Rep. NASA TM-107762; 1993.
[25] C. Borgnakke, Larsen PS. Statistical collision model for Monte Carlo simulation of polyatomic gas mixture. Journal of Computational Physics 18 (1975), 405–420.